Theor Appl Climatol (2013) 113:529–547
DOI 10.1007/s00704-012-0800-1

ORIGINAL PAPER

Numerical investigations of extreme winds over Switzerland during 1990–2010 winter storms with the Canadian Regional Climate Model

Christophe Etienne · Stéphane Goyette · Charles-Antoine Kuszli

Received: 9 June 2012 / Accepted: 12 November 2012 / Published online: 1 December 2012

Abstract This study reports on the ability of the Canadian Regional Climate Model to simulate the surface wind gusts of 24 severe mid-latitude storms in Switzerland during the period 1990–2010. A multiple self-nesting approach is used, reaching a final 2-km grid which is centred over Switzerland, a country characterised by complex topography. A physically-based wind gust parameterization scheme is applied to simulate local surface gusts. Model performance is evaluated by comparing simulated wind speeds to time series at weather stations. While a number of simulated variables are reproduced in a realistic manner, the surface wind gusts show differences when compared to observed values. Results indicate that the performance of this parameterization scheme not only depends on the accuracy of the simulated planetary boundary layer, the vertical temperature, wind speed and atmospheric humidity profiles, but also on the accuracy of the reproduction of the surface fields such as temperature and moisture.

1 Introduction

Intense mid-latitude cyclones forming over the North Atlantic Ocean produce winds that may be amplified by strong gusts over various regions of Western Europe. These storms, associated with extra-tropical cyclones, can assume a large variety of forms depending on the background flow in which they are embedded (Holton 2004). Deep cyclones are associated with strong pressure gradients and have the potential to induce weather extremes, characterised by strong winds over maritime and continental areas (e.g. von Storch and Weisse 2008).

As they often stretch over large geographical areas, windstorms are listed among major natural hazards in Europe (Beniston et al. 2007). In the past decades, a number of intense storms have had catastrophic consequences in terms of human lives, damage to forests and to infrastructures in Europe. Associated economic losses were very important, notably for the December 1999 storms (12 billion US$, Bresch et al. 2000; MunichRe 2001). In Switzerland, the number of winter storms does not show a clear temporal trend (Schiesser et al. 1997) but winter storms strongly impacted forests (Usbeck et al. 2010). Studies highlighted the increase of economic losses due to wind storms during the twentieth century, mainly related to economic and demographic growth (Barredo 2010). An increase of monetary losses is projected in the course of the twenty-first century, based on simulated winds predicted in future warmer climates (e.g. Della-Marta et al. 2010; Schwierz et al. 2010).

Economic loss models have been developed and applied to estimate losses associated to strong winds and to assess risk-prone areas (Heneka and Ruck 2004). They generally take into account the meteorological data describing the wind storm—essentially the maximum wind speeds—and the spatial distribution of insured values to compute monetary losses (e.g. Klawa and Ulbrich 2003; Heneka et al. 2006). In these models, an empirical cubic relationship was found appropriate between the economic losses and the input wind speeds. These wind speeds are provided either by observations recorded at weather stations, or by outputs from numerical models of weather or climate. In

C. Etienne (✉) · S. Goyette · C.-A. Kuszli
Climatic Change and Climate Impacts Group,
Institute for Environmental Sciences, University of Geneva,
Battelle/D, chemin de Drize 7,
1227 Carouge, Geneva, Switzerland
e-mail: christophe.etienne@unige.ch

S. Goyette
e-mail: stephane.goyette@unige.ch

C.-A. Kuszli
e-mail: charles-antoine.kuszli@unige.ch

Switzerland, although the meteorological network is well developed with more than a hundred stations covering a surface of roughly 42,000 km^2, the very irregular and complex landscape makes it difficult to reliably interpolate wind observations across the country (Tveito et al. 2008) to provide accurate spatial distributions of wind speeds as input for loss models (Etienne et al. 2010). Therefore, there is a need to assess as accurately as possible the meteorological aspects of extreme wind storm events with a fine spatial scale.

The prospect of climate change has brought weather and climatic extremes into sharper focus, especially regarding their impacts on human activities, infrastructures and the environment (Beniston et al. 2007). The impacts of climate change on the generation of cyclones in the North Atlantic Ocean, and their passage over Western Europe, is a matter of continuous analysis and investigation (e.g. Lambert and Fyfe 2006; Leckebusch et al. 2006; Pinto et al. 2009a). Intensification in the storm-track climate in the North Atlantic from the mid-1970s to the mid-1990s is reported by Schmith et al. (1998). Investigations are made to assess whether that positive trend will continue or not in the future (Fischer-Bruns et al. 2005; Bengtsson et al. 2006). In a recent study by Wang et al. (2009), storminess is displaying strong differences between the North Sea area and other sectors of the northeast North Atlantic Ocean. In particular, winter storminess showed an unprecedented maximum in the early 1990s in the North Sea area and a steady upward trend in its north-eastern part, while it appears to have declined in the western part of the region. Part of the storminess phenomenon has been related to the North Atlantic Oscillation (NAO) natural variability (WASA group 1998). It is well recognised that the NAO influences the changes of surface westerly flows across the North Atlantic into continental areas (Stephenson et al. 2002). At present, the understanding of current and future changes in extratropical storm activity is a matter of great interest and further studies are needed to investigate the trends in terms of storms tracks, frequencies and intensities, as well as their further impact inland (Lambert et al. 2002; Leckebusch and Ulbrich 2004; Raible et al. 2008; Pinto et al. 2009a; Ulbrich et al. 2009).

Numerical models have proven to be useful for the simulation of extreme wind events (Goyette et al. 2001, 2003). Regional weather and climate models have shown genuine capability for estimating atmospheric processes at fine spatial scales and obtain useful simulations of wind storms (e.g. Benoît et al. 1997; Klawa and Ulbrich 2003; Al-Yahyai et al. 2012). A multiple self-nesting technique is currently used to downscale atmospheric circulation at very high resolution (Goyette 2008). But as flow fields result from non-linear interactions, gusts remain difficult to reproduce when parameterized as subgrid-scale processes.

Early investigations aiming at diagnosing windgust speeds were obtained from sustained wind speed using gust factors (Durst 1960; Wieringa 1973). The gust factor is defined as the ratio of the maximum gust speed to the sustained wind speed, and its value may depend on the measure for sustained wind speed, the magnitude of the wind speed, altitude and topographical features, and the types of atmospheric circulation (Ágústsson and Ólafsson 2004; Jungo et al. 2002). More general models have also been proposed, in which the gust speed is diagnosed as a function of the wind speed with spatially varying parameters (e.g., Etienne et al. 2010). Thereafter, as windgusts are manifestations of turbulence, two approaches to parameterize them were developed and applied in numerical models for weather and climate. The first one computes the non-convective gust speed as a function of the lowest model-level resolved winds, or diagnosed winds at some level between the surface and the lowest model level (e.g. 10 to 30 m), combined with a measure of the intensity of the turbulence in the lowest atmospheric layer (Nielsen and Petersen 2001; Schulz 2008). The second, mainly applied for mid-latitude storms, accounts for the vertical structure of the atmosphere in the planetary boundary layer (PBL) where surface gusts result from the downward deflection of turbulent air parcels (Brasseur 2001). As an alternative to these deterministic approaches, the probabilistic nature of wind gusts has also been recently developed and investigated to locally reproduce strong winds (Born et al. 2012; Thorarinsdottir and Johnson 2012). Both the deterministic and the probabilistic approaches have shown genuine skill to reproduce the windgusts at the surface.

The wind gust parameterisation developed by Brasseur (2001) will be used in this study. This scheme performed reasonably well under various types of wind events and topography. It was initially developed for "off-line" diagnostics of wind gusts, i.e. as a post-process using model outputs archived at regular time intervals. It has been applied over the flat terrain of Belgium (Brasseur 2001) and over the rougher terrain in Iceland (Ágústsson and Òlafsson 2009). It was also implemented and tested in several regional climate models (RCMs) and numerical weather predictions (NWPs) for "on-line" diagnostics using flow fields and other information available at each time step, including the Canadian Regional Climate Model (CRCM), which was applied to the complex terrain of Switzerland and the flat topography of Belgium (Goyette et al. 2003), It was furthermore investigated in Germany using the atmospheric mesoscale model FOOT3DK (Pinto 2009b), where it showed genuine ability during storms. Also, Belŭsić and Klaić (2004) successfully employed this parameterisation to reproduce the strong gusts of bora winds in Croatia, and Ólafsson and Ágústsson (2007) investigated a corner wind and a

downslope windstorm in Southeast Iceland, which they referred to as a "warm bora".

This paper aims to analyse the ability of the CRCM to reproduce a set of 24 extreme winter storms events and their associated strong winds over Switzerland on a 2-km surface computational grid. These 24 intense windstorms, which occurred during the 1990–2010 period, are first simulated over a large computational domain to capture the atmospheric structures at the synoptic scale. A multiple-downscaling technique is then used to reach the 2-km grid spacing, where the wind gust parameterization is implemented to simulate maximum wind speeds. The model performance is tested by comparing simulated output to observations; synoptic scale patterns are compared with weather charts at mean sea level and at the 500-hPa levels, and a comparison of simulated daily maximum wind speeds with station observations for various regions of Switzerland that exhibit different topographic conditions is performed.

The following sections include a short description of the study area and of the local meteorological measurements provided by weather stations. The selection and the characteristics of the 24 storms that struck Switzerland are then described. Next, a description of the numerical climate model and the wind gust parameterization is given. The wind outputs of the model simulations are discussed in details and compared to both synoptic and surface local observations. The observed and simulated vertical profiles at the Payerne aerological station are further analysed in order to evaluate the performance of the wind gust parameterization scheme.

2 Data and numerical model

2.1 Study area

The topography of Switzerland is complex, with a relatively low and narrow mountain range in the north called the Jura, and high mountain peaks in the Alps in the south that often exceed 4,000 m above mean sea level. In the centre, stretching from east to west between these two mountain ranges, is a relatively flat area commonly referred to as the "Swiss Plateau". Mountainous areas occupy more than 60 % of the surface of the country; therefore sharp gradients of elevation are frequent. The Alps act as a climate barrier, distinguishing the northern part, under the influence of both Atlantic and continental air masses, from the southern part influenced by the Mediterranean Sea.

Switzerland experiences many large-scale-driven wind regimes that may induce numerous local winds influenced by topography, such as the "Bise" (Wanner and Furger 1990), the "Joran" (Bohle-Carbonell 1991) and north and south Foehn. The latter is induced by the crossing of a depression through the Alps, and flows from the south-east (Hoinka 1985). The "Bise" is a name given to cold north-easterly winds in the Swiss Middleland (the region between the Jura and the Alps), which are driven by an anticyclone building to the northwest of the Alps. Schüepp (1978) compiled over 40 different climate types across the Alps. In Switzerland, as in most of central Europe, the most damaging historical storms generally occurred during the winter (e.g. Pfister 1999; Lambert and Fyfe 2006; Ulbrich et al. 2009).

2.2 MeteoSwiss data

Switzerland has a dense network of automatic weather stations where observations have been compiled and made available every 10 min since 1981, providing reliable and quality-checked data in digital format (Bantle 1989; Begert et al. 2005). Weather stations are located in a variety of locations, from 200 to over 3,500 m a. s. l., providing a wide spectrum of the various topographic conditions across the country (Fig. 1d). MeteoSwiss also provides vertical atmospheric profiles at the aerological station of Payerne (46.8° N, 6.9° E, 490 m a.s.l.). These vertical radiosoundings, which have already been investigated to analyse near-alpine wind conditions (e.g. Furger 1992; Henne 2005), are part of an international effort to analyse atmospheric processes in three dimensions and are launched simultaneously every 12 h in the world (0000 and 1200 UTC).

2.3 Lake temperature

Surface temperatures are important for NWPs as well as for RCMs in order to accurately compute atmospheric flow fields (Pielke 2002). They have a notable influence on the latent and sensible heat fluxes (Abdella and McFarlane 1997). The types of surface have also an impact on boundary layer flows, for example on the physical shear stress (Mitchell et al. 1985). Each point of the surface grid is assigned to either solid ground or open water. For the 2-km CRCM land surfaces, surface characteristics are inferred from the Ecoclimap dataset (Champeaux et al. 2005), which provides European land-use information at a 1-km scale. Roughness length (z_o), albedo (α) as well as a number of other thermal and hydrologic parameters are associated to each land-use class.

For the inland freshwater lakes located in Switzerland, surface temperature data is provided by different cantons or research institutions of Switzerland. Typically, monthly or two monthly lake surface temperature data are available for most of the major lakes of the studied area (Leman, Brienz, Thun, Bienne, Morat and Neuchâtel) and are used for the

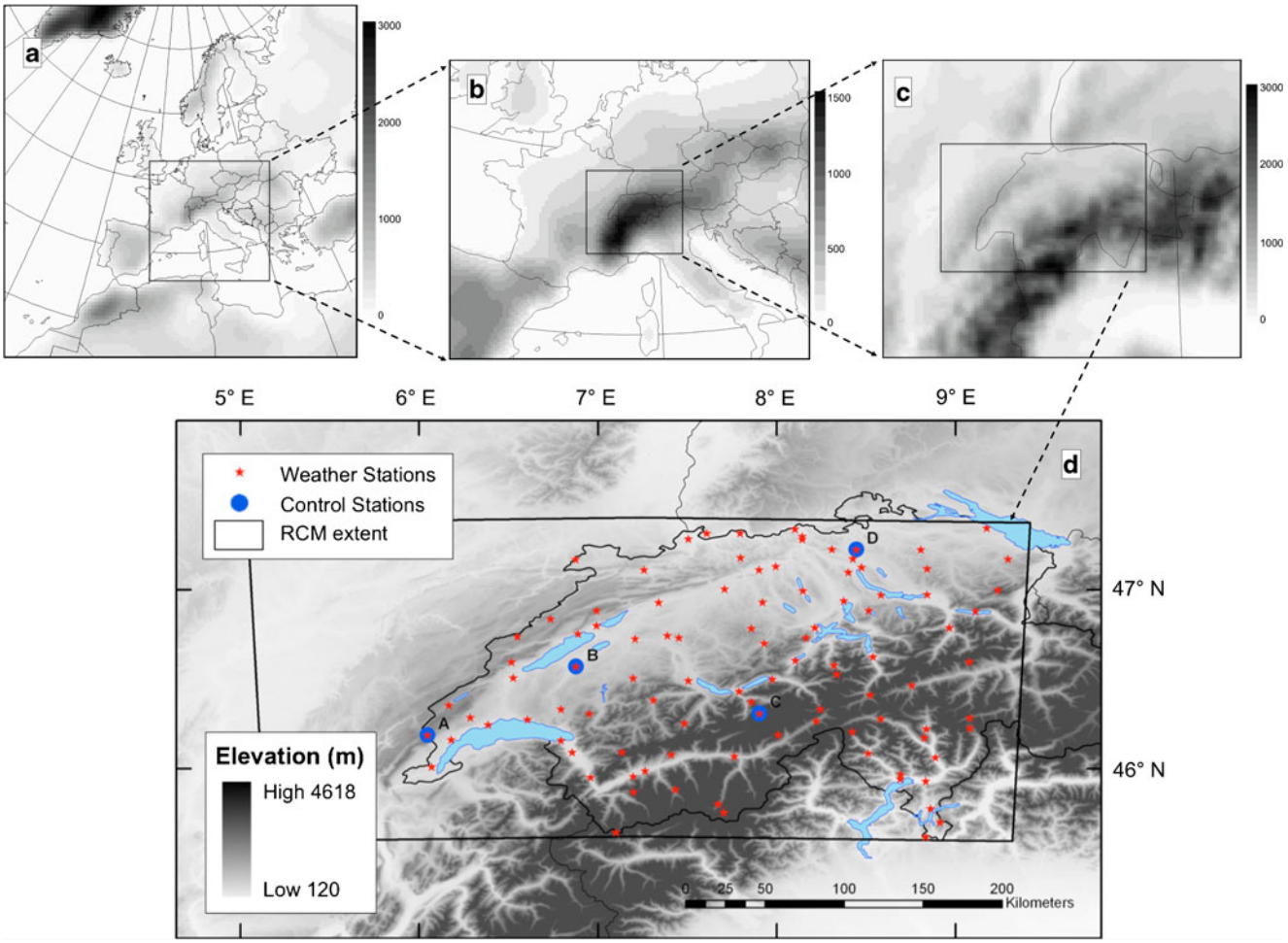

Fig. 1 The four computational domains used in the multiple self-nesting methodology showing the surface topography (metres) in *grey tones*, the 60-km grid (**a**), the 20-km grid (**b**), the 5-km grid (**c**) and the 2-km grid (**d**), the latter being shown together with the Swiss borders. The surface extent of the 2-km grid is roughly 360 km wide and 220 km long. The 100 weather stations are shown, as well as the four control stations where the 2-km CRCM simulated winds are compared to observations: La Dôle (*A*), Payerne (*B*), Jungfraujoch (*C*) and Zürich (*D*). Vertical profiles are provided and further compared only at the Payerne aerological station (*B*)

numerical simulations of the 24 storms with the 2-km CRCM. Temperatures generally range from 6 to 8 °C in December, decrease in January and February to get close to 5 °C; values can occasionally drop to approximately 4 °C for the smaller lakes. Measurements are provided for a single point per lake, except for Lake Geneva which has two. Spatial interpolation of these two input values is made for the entire lake to assess the surface temperatures. Lake surfaces have prescribed surface roughness height and albedo values, and hence have their own specific influence on local flows.

Surface temperature data were not available for the lakes Zürich, Zug and Lucerne. Lakes Constance and Maggiore lack surface temperature data as well, but they are located on the edge of the computational grid, in the buffer zone of the 2-km CRCM (Fig. 1). Possible frozen lake surfaces during winters were not computed and therefore not taken into account in the simulations.

2.4 Storm events

Twenty-four storms were investigated in this study (Table 1). These were detected by analysing extreme wind speed statistics from the historical weather station records. Daily maximum wind speeds from the 1990–2010 period were extracted for all meteorological stations, and local 98th percentiles of these values were calculated for each station. Storm events were considered when these local thresholds were simultaneously exceeded at a minimum of five stations, and when they caused economic loss. This selection led to a list of 24 events during the past two decades. For Switzerland, winter storms Vivian on 27 February 1990 (Schraft et al. 1993) and Lothar on 26 December 1999 (Bresch et al. 2000) were the most devastating events of the last two decades. The Vivian storm struck particularly the Swiss Alps with a record gust of 74.5 ms^{-1} recorded at the Grand St. Bernard station (45.87°N, 7.17°E), causing

major destruction to the transportation sector and devastating important tracts of forests (Schüepp et al. 1994). The Lothar storm hit Switzerland more globally, causing severe damage to infrastructures and forests, with total economic losses estimated above 10 billion Euros. More recently, in late February 2010, the Xynthia storm also caused important losses, especially in France, related in part to the exceptional storm surges along the Atlantic coast. The remaining 21 storms caused less significant damage. Economic loss is estimated for the same 24 wind storms for the Canton of Vaud, in Western Switzerland (Etienne and Beniston under review).

Most of the storms are induced by westerly flows (including Vivian and Lothar), but some were induced by south winds-as was the case for storm Xynthia which generated strong Foehn-type winds in Switzerland or north-east or easterly flows that led to strong "Bise" events. The daily North Atlantic Oscillation Index (NAOI), which is calculated following the methods described in Barnston and Livezey (1987) and available at the National Oceanic and Atmospheric Administration (http://www.noaa.gov), is also provided for each storm. Positive NAOI generally matches strong winds induced by westerly flows, negative NAOI values generally correspond to south Foehn events or south-west winds, as well as easterly and north-easterly flows.

2.5 The atmospheric model: the Canadian RCM

The numerical model used in this study is the Canadian Regional Climate Model (CRCM). The main features of this version of the CRCM are described in Laprise et al. (1998) and Caya and Laprise (1999), and a number of applications can be found in Antic et al. (2005), Denis et al. (2002), Goyette et al. (2000), Laprise et al. (2003) and Martynov et al. (2012). In the following, the lateral and uppermost nesting technique consists of driving the CRCM with a time series of atmospheric flow fields extracted from National Centers for Environmental Prediction (NCEP)–National Center for Atmospheric Research (NCAR) reanalyses (Kalnay et al. 1996), namely pressure, temperature, water vapour and horizontal wind, which are provided six hourly on a 2.5°×2.5° grid with 17 vertical levels for all variables except for specific humidity which has 8. The technique also uses a nudging procedure to drive the large-scale flow (cut-off wave length scale of 1,400 km) over the entire domain. This technical method is meant to keep the large-scale atmospheric flow fields in the CRCM computational domain close to the ones of the driving reanalysis fields. The strength of the nudging tendency increases from 500 hPa for the wind fields and 50 hPa for temperature, to a maximum at the model lid (Plummer et al. 2006; Alexandru et al. 2009). Consequently, the nudging has practically no effect on the smaller computational domains when their sizes are smaller than the cut-off length scale.

This study employs the self-nesting that allows the flow fields to be simulated at very high resolution in a stepwise manner (Fig. 1). Prescribed sea surface temperatures, sea-ice, topography, land-use and other fixed geophysical fields from Wilson and Henderson Sellers (1985) are interpolated onto the 60- and 20-km CRCM computational surface grids. The lower boundary conditions of the 5- and 2-km CRCM computational grids are prescribed from high-resolution dataset (Masson et al. 2003), and on the 2-km surface grids many lakes are resolved and surface temperatures are derived from observations (Section 2.3). The overall nesting procedure is designed to be one-way, as there are no feedbacks from the fine scales to the large scales.

2.6 Wind gust parameterization

In order to simulate the strong winds at the anemometer level, the wind gust parameterization of Brasseur (2001) has been implemented in the CRCM physics package (Goyette et al. 2003; Goyette 2008). This approach assumes that surface gusts result from the downward deflection by turbulent eddies of air parcels flowing higher in the PBL. The wind gust estimation (WGE) method takes into account the mean wind, the turbulent structure of the atmosphere and the buoyant energy in the PBL. This physically-based parameterization as detailed in Brasseur (2001), taking into account the modifications suggested by Burk and Thompson (2002), and acknowledged in Brasseur et al. (2002), is as follows:

$$\frac{1}{z_{\mathrm{p}} - z_{10\mathrm{m}}} \int_{z_{10\mathrm{m}}}^{z_{\mathrm{p}}} \mathrm{TKE}(\mathrm{z})\,\mathrm{d}\,\mathrm{z} \quad \geq \quad g \int_{z_{10\mathrm{m}}}^{z_{p}} \frac{\Delta\theta_{\mathrm{v}}}{\Theta_{\mathrm{v}}}(z)\,\mathrm{d}\,\mathrm{z} \qquad (1)$$

where TKE is the turbulence kinetic energy, z_{p} the parcel where the gust is originating, $z_{10\mathrm{m}}$ is the anemometer level located at 10 m above the surface, $\Delta\theta_{\mathrm{v}}$ is the virtual potential temperature between the environment at height z_{10} and a parcel adiabatically displaced from z_{p} to $z_{10\mathrm{m}}$, and Θ_{v} the potential temperature at height z_{p}, with $z_{10\mathrm{m}} \leq z_{\mathrm{p}} \leq z_{\mathrm{PBL}}$. The gust speed, G, is estimated as the maximum wind speed found in the PBL as:

$$G = \max\left[\sqrt{u^2(z_{\mathrm{p}}) + v^2(z_{\mathrm{p}})}\right] \qquad (2)$$

with z_{p} satisfying Eq. 1. For a given time step, if the condition stated in Eq. 1 is not satisfied, the value of G is then fixed to the anemometer-level wind speed as the lower bound. Consequently, the gust values are always greater or equal to the anemometer wind speed. TKE is not computed prognostically in the CRCM, therefore the parameterization adopted to compute this quantity is based on the "level 2"

turbulence second-order closure of Mellor and Yamada (1974) as detailed in Goyette et al. (2003). TKE in (1) is determined diagnostically as follows:

$$\mathrm{TKE} = \frac{1}{2}\left\{ \mathrm{B_1\, l_m}\left[\mathrm{K_h}\left|\frac{\partial \mathrm{V_H}}{\partial \mathrm{z}}\right|^2 (\mathrm{Pr} - \mathrm{Ri})\right]\right\}^{\frac{2}{3}} \tag{3}$$

where B_1 is an empirical parameter fixed at 16.6 (Mellor and Yamada, 1982), l_m the master mixing length (Blackadar 1962) tending asymptotically to 100 m, $\mathrm{Pr}=K_m/K_h$ the turbulent Prandtl number as a function of the ration between the turbulent coefficients for momentum, K_m, and that for heat, K_h, and z is the height above the local terrain. The turbulent coefficients are those used in the CRCM and defined in McFarlane et al. (1992):

$$(K_m, K_h) = l_m^2 \left|\frac{\partial V_H}{\partial z}\right| [f_m(\mathrm{Ri}), f_h(\mathrm{Ri})] \tag{4}$$

where $V_H=[u, v]$ the horizontal components of the wind, f_m and f_h are dimensionless functions of the atmospheric stability measured by the local Richardson number defined as:

$$\mathrm{Ri} = \frac{\frac{\mathrm{g}}{\theta}\frac{\partial \theta}{\partial z}}{\left(\frac{\partial \mathrm{V_H}}{\partial z}\right)^2} \tag{5}$$

with θ the potential temperature and g the acceleration due to gravity.

3 Methodology

The main aim of this paper is to assess the ability of this CRCM model configuration to simulate past storm events over the complex terrain of Switzerland, and to evaluate the ability of the current wind gust parameterization to simulate the strong winds that occurred during these windstorms. To estimate the model performance, the synoptic conditions provided by NCEP–NCAR reanalysis data that drives the 60-km CRCM have been systematically compared and validated with the MeteoSwiss weather bulletins, and the simulated surface wind speeds compared to local observations provided by meteorological stations managed by Meteo Swiss. In a subsequent step, to assess the model's ability to simulate the flow fields, simulated temperature and wind speed vertical profiles have been compared to the observed profiles derived from radiosoundings made at the Payerne aerological station in Switzerland.

3.1 Model configuration and setup

The high-resolution modelling of wind fields, including the gusts, is achieved through the multiple self-nesting capabilities of the Canadian CRCM. It has already been demonstrated in a number of studies that very high-resolution simulations that rely on larger-scale information, either GCM outputs or reanalysis data, cannot directly be downscaled without further intermediate steps (e.g. Benoît et al. 1997). These steps aim to decrease the computational grid spacing in a stepwise manner, where the ratio between two successive grid meshes must be chosen between 3 and 5. As a first step, the temperature, specific humidity and horizontal wind components of the reanalyses are driving 60-km CRCM during a 30-day periods starting two weeks prior the storm events. Then, the flow fields from these are driving the 20-km CRCM during the same period as the 60-km CRCM. Then, self-nesting the CRCM with 20-, 5-and 2-km grids proceed in a similar manner as shown in Fig. 1, but for shorter time periods. As we proceed to higher horizontal resolution, the number of vertical levels increases and the time steps decreases to warrant numerical stability. For instance, the 2-km CRCM employs a 180×100 grid mesh, 46 levels in the vertical, including 27 levels below 5,000 m, and a time steps of 15 s. Many details and model configuration found in this study are similar to that of Goyette (2001) and Goyette (2008). However, compared to Goyette (2008), the 2-km computational domain has been shifted slightly to the West to avoid the western Swiss boundaries to lie too close to the grid western boundaries.

The wind gust parameterization of Brasseur (2001) is implemented in the 2-km CRCM only; this horizontal resolution is required to resolve some of the topographical details of the Swiss Alps. The PBL behaviour and gusts distribution are also better represented with a high vertical resolution. In the 2-km CRCM simulations, larger Swiss lakes are resolved on the surface grid; consequently lake surface temperature distributions have been prescribed as constant values over time during the 5-day periods centred on the time when the strongest winds were recorded. The initial conditions are derived first by interpolating the 5-km CRCM surface temperature and moisture fields onto the 2-km surface grid. Then, the simulations are spun up by running twice the CRCM over these 5-day periods for each storm using surface fields computed at the last time step as initial conditions for new runs.

4 Results

In this section, outputs of the numerical simulations are analysed and compared to observations recorded by the MeteoSwiss stations. Quality of the wind gust parameterisation is assessed by examining daily maximum wind speeds and wind gust time series. As surface atmospheric pressure is linked to the evolution of the windstorms, they are also considered and analysed. Three events—one from each of the three different storm types listed in Table 1—are

Table 1 List of the 24 storms investigated in this study including the given storm name when available, the day of occurrence, the corresponding daily North Atlantic Oscillation index (NAOI) and the major wind directions or local wind designation in Switzerland

Storm number (given name)	Storm date	NAOI	Synoptic conditions (regional wind system in Switzerland)
1 (Vivian)	27 February 1990	1.12	Westerly flow
2	21 December 1993	1.04	Westerly flow
3	28 January 1994	0.21	Westerly flow
4	26 January 1995	0.06	Westerly flow
5	16 February 1995	1.48	Westerly flow
6	13 February 1996	0.33	Westerly flow
7	11 November 1996	−0.67	Southerly flow (Foehn)
8	13 February 1997	0.92	Westerly flow
9	17 December 1997	−2.14	Southerly flow (Foehn)
10	05 January 1998	0.63	Westerly flow
11	19 January 1998	0.40	Westerly flow
12	12 December 1999	1.10	Westerly flow
13 (Lothar)	26 December 1999	1.33	Westerly flow
14	16 February 2000	1.24	Westerly flow
15	06 November 2000	−1.41	Southerly flow (Foehn)
16	14 December 2001	−1.54	North-easterly flow (Bise)
17	02 January 2003	−0.05	Westerly flow
18	12 January 2004	0.69	Westerly flow
19	23 November 2005	−0.49	North-easterly flow (Bise)
20	01 January 2007	0.80	Westerly flow
21	03 December 2007	0.43	Westerly flow
22 (Klaus)	23 January 2009	0.72	Westerly flow
23	10 February 2009	−0.37	Westerly flow
24 (Xynthia)	28 February 2010	−0.28	Southerly flow (Foehn)

investigated in details. For the comparisons with observations, each weather station was matched to the corresponding closest grid point of the CRCM mesh. As the CRCM grid spacing is of 2 km, the matching grid points are located no further than 1.4 km away from each individual station. Although they are essential steps during the downscaling procedure to drive 2-km CRCM, the 20 and 5 km runs have been systematically checked but are not analysed and discussed further in this paper.

4.1 Synoptic conditions during the occurrence of the storms

As the 60-km CRCM is embedded in the NCEP–NCAR-gridded reanalyses to simulate past events, storm-relevant variables such as the mean sea-level pressure (p_{msl}) and the height of the 500 hPa level (ϕ_{500}) have been systematically compared to the corresponding synoptic weather charts valid at 1200 UTC provided by MeteoSwiss on a daily basis. In many of these windstorms, the primary cyclone or the secondary waves to which the strong winds are associated are mainly located to the NNE to NNW of Switzerland. In other words, the strong winds are located to the southern edges of these mid-latitude cyclones; Fig. 2a, b displays the p_{msl} and ϕ_{500} of one of these on 1200 UTC 26 January 1995. At the 500 hPa level, geopotential height show steep north–south gradients inducing strong west–east components of the horizontal wind velocity over the Swiss territory. Four storms produced surface winds from the SSW sector and the low pressures were located further south off the coast of Brittany in France and the high pressures located in eastern Europe; Fig. 2c, d shows the p_{msl} and ϕ_{500} of one of these on 1200 UTC 17 December 1997. The geopotential height of the 500 level the steep north–south gradients is located further west compared to the storm producing eastward surface flow. Two storms produced surface winds from the northeast. Figure 2e and f show the p_{msl} and ϕ_{500} for 1200 UTC 23 November 2005. The position of the primary cyclone, of the secondary waves, and that of the main wind direction at the surface and at the 500-hPa level may differ for each individual storm, however.

4.2 Statistics for all stations applied to 3 typical storms

To obtain a quantitative overview of the 2-km CRCM ability to reproduce strong winds, hourly simulated values, the maximum gusts, the mean of these maximum gusts and the mean pressure are compared to observations for each storm at all stations (Fig. 3). Hourly values are considered for a minimum of days: 1 day before and 1 day after each storm date. To assess uncertainty, bootstrap techniques are applied to all series by calculating the R^2 coefficients from 1,000 random datasets, and an overall mean R^2 is then calculated. The Spearman rank coefficient (ρ) is also plotted.

For pressure values, correlation coefficients of above $R^2=0.75$ are found, with observed and simulated values being fairly well aligned about the 1:1 line (Fig. 3, right graphs). Values for the wind maximum speed averages are mostly below 20 $m\,s^{-1}$ for all storms (Fig. 3, middle graphs). CRCM values generally underestimate observations, except for the storm of 17 December 1997. The R^2 coefficient is less than 0.5, and no apparent relationship between observed and simulated mean gusts can be detected. The same conclusions can be made for the maximum gusts at all stations, as no clear trend is observed and coefficients are low (Fig. 3, left graphs). Simulated values are not always overestimating observations, as some points are below and others above the perfect match, except for the wind gusts of the 17 December 1997 storm which are generally overestimated by the model.

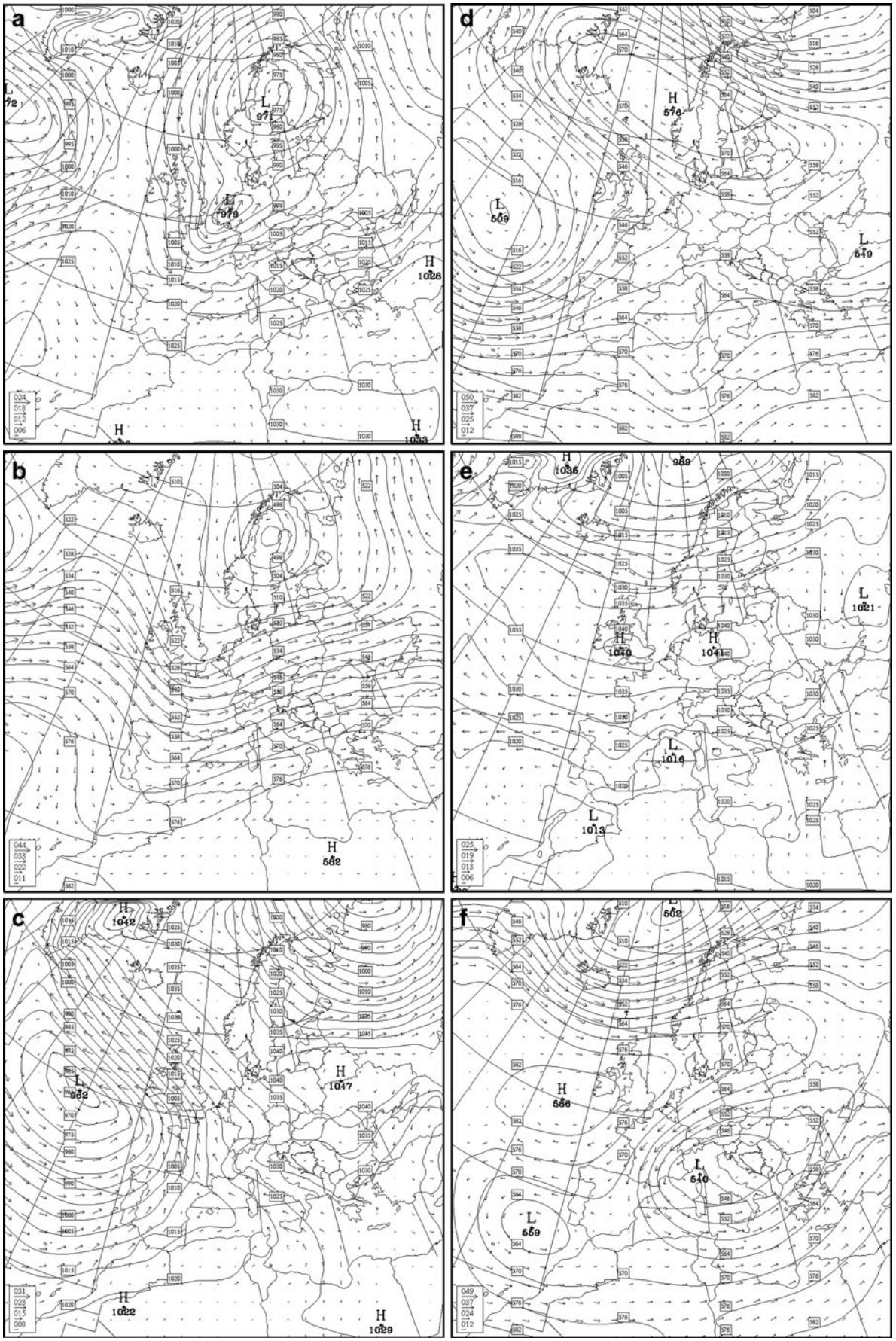
a
b
c
d
e
f

◀ **Fig. 2** **a** Mean sea-level pressure, p_{msl}, (contours 5 hPa) and horizontal wind vectors (magnitudes in metre per second in *insets*) for 1200 UTC 26 January 1995, as simulated by the 60-km CRCM; this is an example of westerly flow conditions in Switzerland. **b** Geopotential heights at the 500 hPa level, ϕ_{500}, (contours 4 dam) and the 500 hPa horizontal wind vectors (magnitudes in metre per second in *inset*) for 1200 UTC 26 January 1995 1200 UTC, as simulated by the 60-km CRCM. **c** Same as **a**, but for the 1200 UTC 17 December 1997. This is an example of southerly flow conditions in Switzerland. **d** Same as **b**, but for 1200 UTC 17 December 1995. **e** Same as **a**, but for the 1200 UTC 23 November 2005. This is an example of north-easterly flow conditions in Switzerland. **f** Same as **b**, but for 1200 UTC 23 November 2005

4.3 Time series at weather stations

The performance of the model was tested in four typical locations (see Fig. 1) by comparing the observed hourly mean pressure and the maximum wind speeds to the 2-km CRCM corresponding simulated time series. Outputs from the closest grid points to each of these stations are plotted and compared to observations for each storm. An example is shown in Fig. 4a for the west winds of storm 4 (26 January 1995). The 2-km CRCM simulated outputs are displayed in

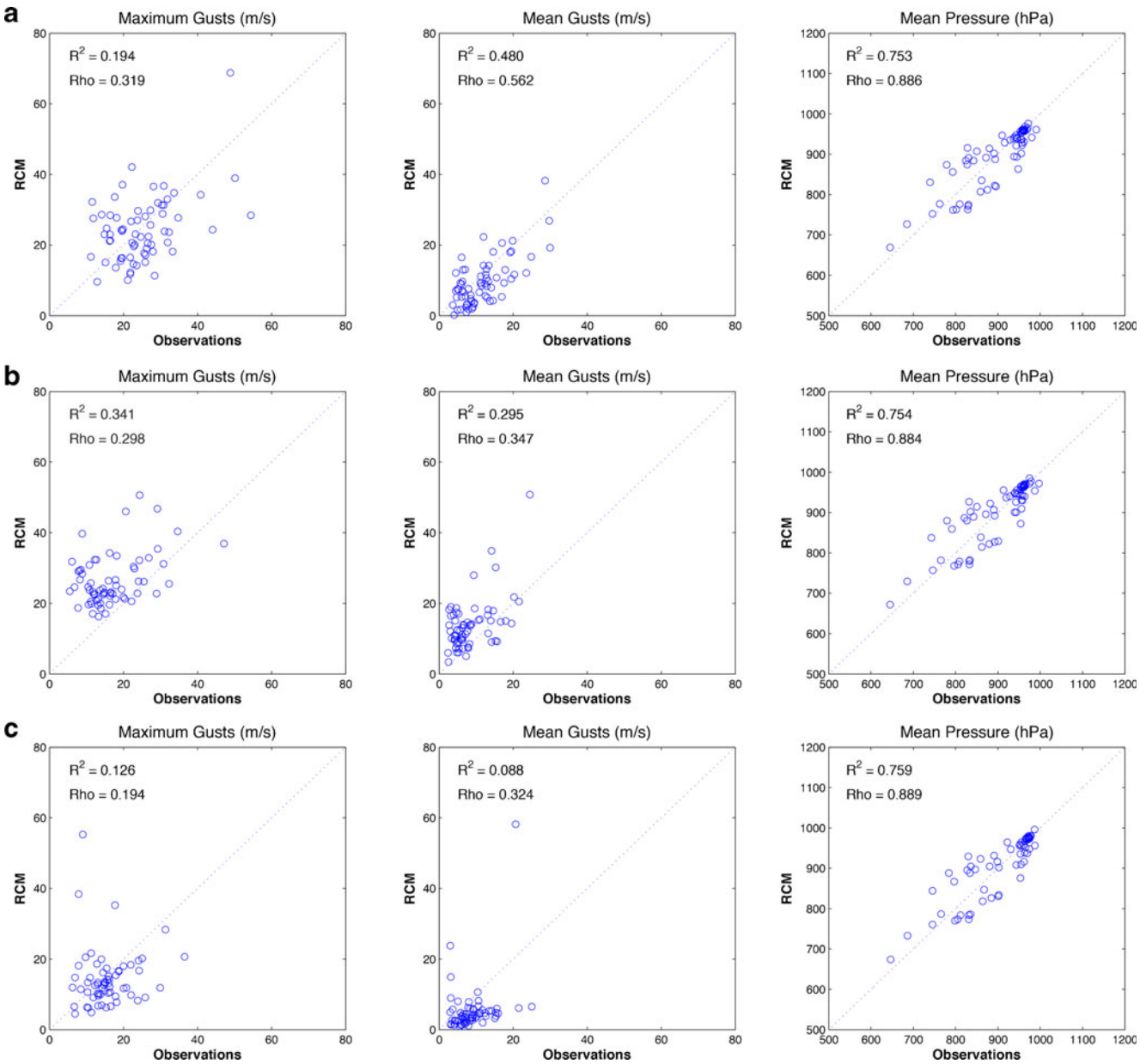

Fig. 3 Scatter plots of the 2-km CRCM outputs to MeteoSwiss observations at all hundred weather stations for storms of 26 January 1995 (**a**), 17 December 1997 (**b**) and 23 November 2005 (**c**). The maximum gusts (*left*), the mean gusts (*middle*) and the mean pressure values (*right*) calculated for 3 days (starting 1 day before and ending 1 day after the storm date) are plotted. Determination coefficients (R^2) and the Spearman's rank coefficients (Rho) are indicated for each scatterplot, as well as the 1:1 line (*dotted line*)

red, whereas the observed data are in blue. For each station, top graphs illustrate the hourly maximum wind speeds (metres per second) and bottom graphs the hourly mean pressure (hectopascal).

For all storms, the simulated 2-km CRCM surface pressure values correspond fairly well to the observed values in Payerne and Zürich, but differ by roughly 70 and 30 hPa for station La Dole and Jungfraujoch, respectively. These gaps may be attributed to the altitude difference between the weather station and the topography resolved on the 2-km CRCM surface grid. The altitude differences are close to zero for the former, but reach 300 and 500 m for the latter. Both simulated and observed pressure values show important variations during the storm event, with amplitudes of roughly 20 hPa.

The wind speeds values shown in Fig. 4a exhibit important variations. The orders of magnitude are generally respected and the mean graph behaviours are similar. For the Jungfraujoch station, both observed and simulated winds show comparable behaviours initially, until the model values overestimate observations and lead to a peak on 28 January 1995. However, the altitude differences may not explain the poor reproduction of the surface wind gusts at that location. The Jungfraujoch weather station located at 3,580 m a.s.l. is often decoupled from the boundary layer so that the parameterization developed to reproduce wind gust at the surface may not be appropriate in its current formulation as is based on the deflection of air parcels flowing in the PBL. At the other three stations, simulated winds hardly reproduce the observations: the time evolution of the curves look similar, but the simulated winds show discontinuities as wind speeds sometimes drop suddenly to values close to zero. These differences will be detailed in the next section. Except for the Jungfraujoch, a decrease in surface pressures is correlated with an increase of wind speeds for all stations,

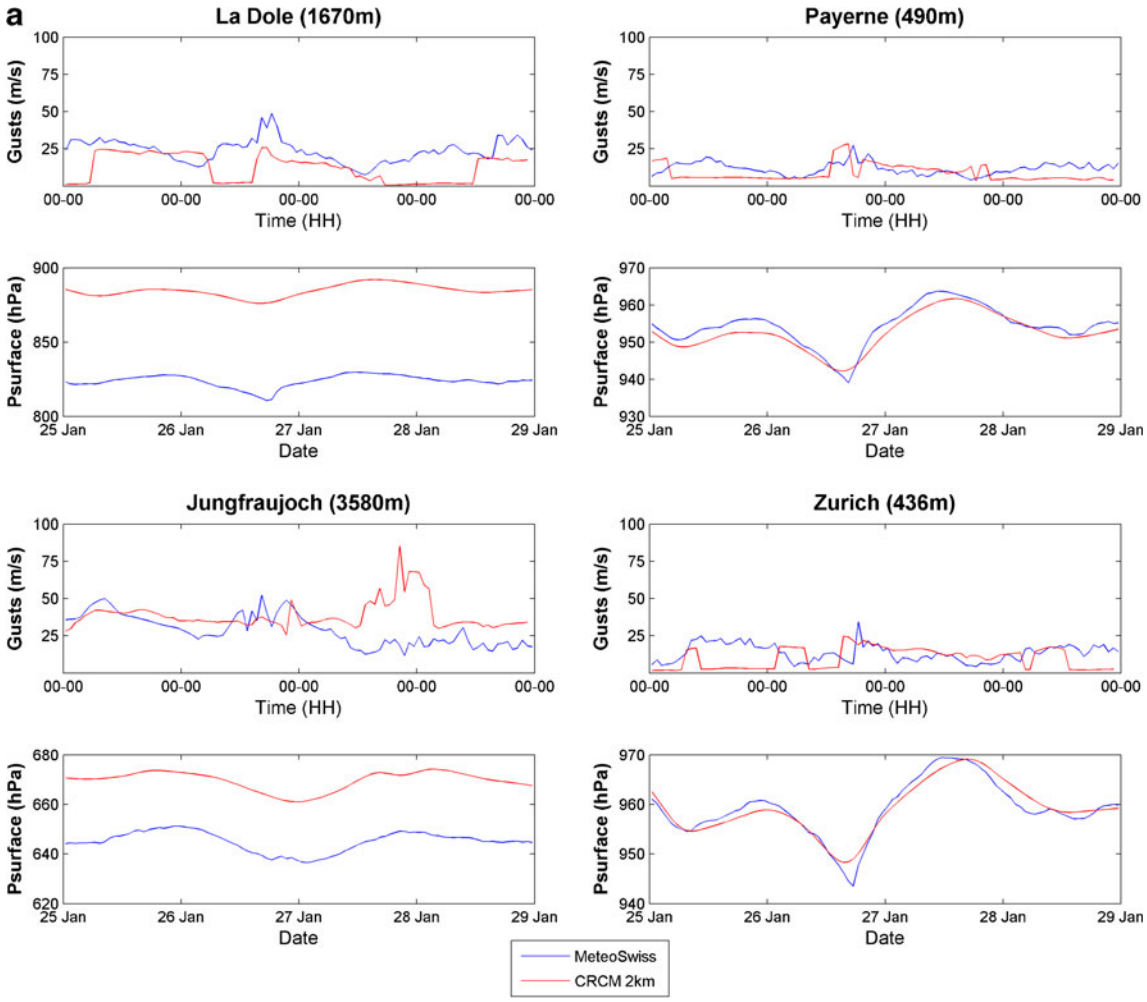

Fig. 4 **a** Example of a comparison of 2-km CRCM outputs for storm 4 (26 January 1995—in *red*) with MeteoSwiss observations of four weather stations (in *blue*). For each station, the hourly wind gusts and the hourly mean pressure values are plotted. The time series are plotted for 3 days, starting 1 day before and ending 1 day after the storm date. **b** Same as **a** but for storm 9 (17 December 1997). **c** Same as **a** but for storm 19 (23 November 2005)

Fig. 4 (continued)

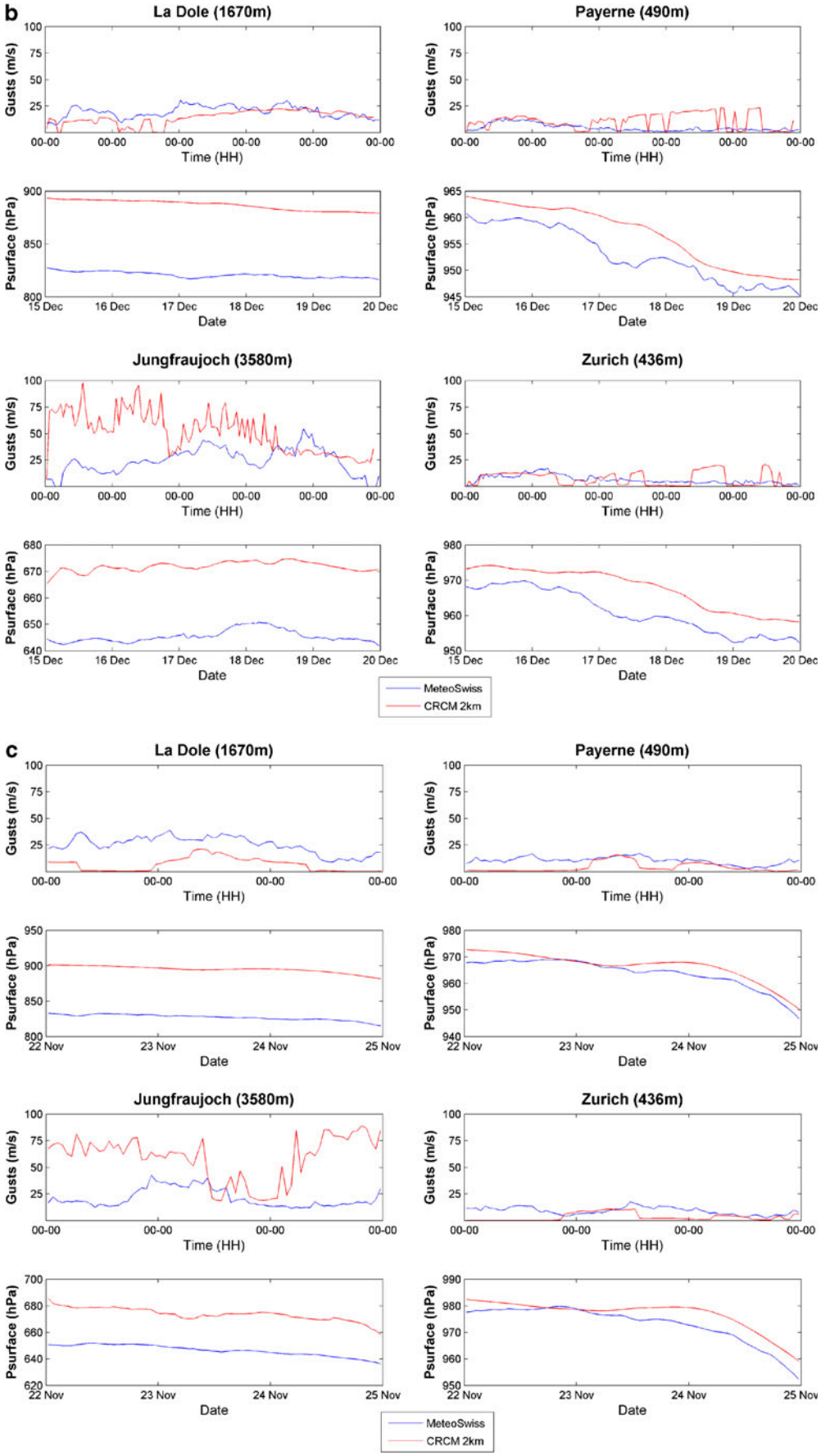

as the strongest winds occur when the lowest pressures are reached.

Figures 4b, c plots the time series for the two other typical storms, the 17 December 1997 (Foehn—storm 9) and the 23 November 2005 (Bise—storm 19). The remarks stated for the analysis of Fig. 4a stand as well, with particular attention to the wind and pressure simulations in the Jungfraujoch. The simulations have failed to reproduce the conditions at that location.

4.4 Vertical profiles analysis

While producing reasonable overall results, the simulated gusts using the Brasseur's parameterization in the CRCM show some discrepancies when compared to observed hourly wind maximum as shown in the previous section. In order to investigate and seek out possible reasons for these discrepancies, a similar parameterization scheme has also been applied to compute the surface wind gusts from observed profiles. These profiles have been compiled from radiosoundings made at the Swiss climatological station Payerne at 0000 and 1200 UTC. These profiles include the horizontal wind speed, a moisture variable, the air temperature and the atmospheric pressure for a number of levels from the surface up to the stratosphere. To re-compute surface wind gusts, all relevant quantities have been projected on the available observation heights. These heights are not equally spaced and may vary in each radiosounding.

Many of these quantities can be evaluated from simulated or observed vertical profiles. These are the horizontal wind speed, $V_H(z)$, the temperature, $T(z)$, a moisture variable such as the specific humidity, $q(z)$, the potential temperature, $\theta(z)$, the atmospheric pressure, $p(z)$, as well as the virtual potential temperature, $\theta_v(z)$. These serve to compute values of Ri, f_m, f_h, K_m, K_m, and then those of Pr and TKE found in Eqs. 1–5. In the CRCM, a number of quantities are available to use at each time step in the Physics routine to carry out all the computations involved these equations. Radiosoundings are available only at 12-hourly intervals, at 0000 and 1200 UTC. For the analysis, the CRCM grid point location to extract the vertical profiles of the archives at those time intervals is selected as the closest in distance to the Payerne station. Then, the application of the Brasseur's scheme to the observed virtual potential temperature and wind profiles shows how this parameterization performs with observations. The comparison and analysis may first be carried out in terms of observed and simulated $V_H(z)$, and $T(z)$ [or $\theta(z)$] prior and during a number of storms to give details on the differences between simulated and observed maximum surface wind speed. Then, the computed surface wind gusts upon applying the observed profiles to the Brasseur's scheme are compared to the observed surface hourly wind maxima.

Many simulated and observed wind and temperature profiles have been analysed and common features became apparent. For example, Fig. 5a shows temperature profiles obtained from a radiosounding at Payerne and computed by the 2-km CRCM on 0000 UTC 25 January 1995, prior to the winter storm induced by westerly flows that occurred on 26 January 1995. The radiosonde went up to approximately the CRCM lid. At this time, the simulated surface maximum wind speed as computed in the 2-km CRCM overestimated the observed hourly maximum wind speed by roughly 10 ms^{-1} (Fig. 5b), but during this day on average, the simulated surface maximum wind speed underestimated the observed hourly maximum wind speed (Fig. 4a). The simulated and observed temperature profiles below the tropopause are in a general agreement: both profiles in the lower troposphere indicate subadiabatic and conditionally stable layers, thus a rather stable atmosphere. The temperature inversion is simulated 600 m above the observed one. In Fig. 5b, an observed low-level wind maximum called a low-level jet (LLJ) located below the temperature inversion is reproduced by the 2-km CRCM but slightly lower than the observed one. In the troposphere, the simulated vertical shear of the horizontal wind speed is not generally as steep as the observed one. In addition, while simulated roughly at the same level as observed, the jet stream is underestimated by more than 14 ms^{-1}. In the model, the Richardson number is close to its critical value in the low levels due to the lapse rate values and the relatively small value of the vertical wind shear. Consequently, the dimensionless functions of the atmospheric stability f_m and f_h produce moderate values of the turbulent coefficients for momentum, K_m, and for heat, K_h. The turbulent Prandtl number is thus not large enough to produce positive values of Pr–Ri, and subsequently that for the vertical integral of TKE, which magnitude is not large enough to overcome the large buoyancy forces produced by the strong static stability, the latter being proportional to the vertical integral of $\Delta\theta_v/\Theta_v$ (Eq. 1). This results in a value of the simulated wind gust, G, equal to the simulated anemometer-level wind speed. The anemometer-level wind speed, a diagnostic quantity computed on the basis of the first model-level resolved wind components and extrapolated down to the anemometer level using a logarithmic profile, is also underestimated because the slope of the extrapolation is a function of the stability which produced a low surface momentum drag coefficient. This bulk-aerodynamic method, described in McFarlane et al. (1992) uses the bulk Richardson number that is slightly positive in the first model layer which produces a relatively low momentum transfer function value upon which the momentum drag depends. Figure 5c shows that the

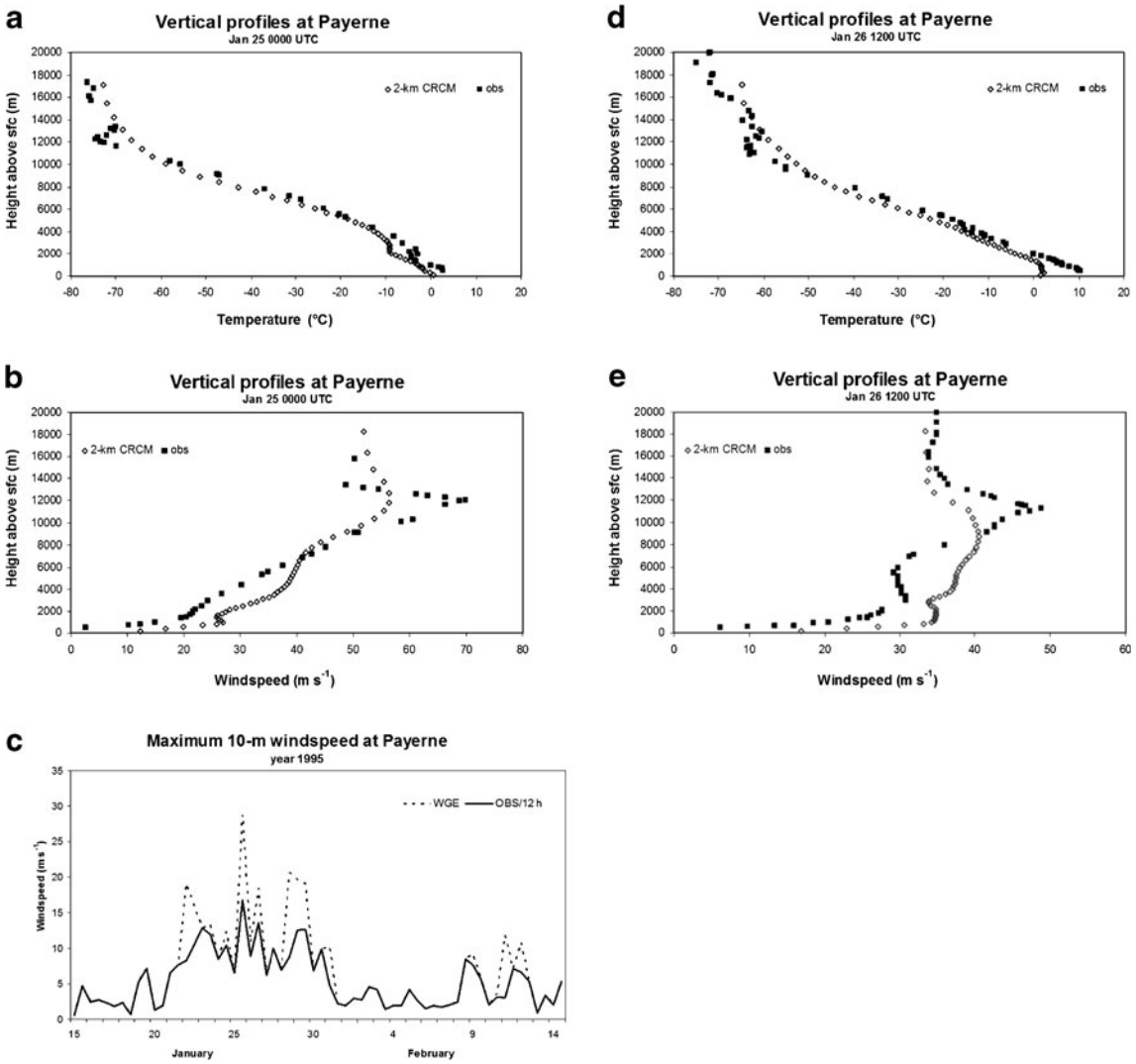

Fig. 5 **a** Observed (*obs*) vertical temperature profiles obtained from a radiosounding at Payerne, Switzerland, on 0000 UTC 25 January 1995 and simulated (*2-km CRCM*) profiles from the closest 2-km CRCM grid point to this station. **b** Same as **a** but for wind speed profiles. **c** Evolution of 12-hourly maximum wind speed at the surface as observed at the Payerne station (*Obs/12 h*), Switzerland, and those computed with the Brasseur's method applied to observed virtual potential temperature and wind speed vertical profiles (*WGE*) for the period 15 January to 15 February 1995. The lower bound of the estimated wind gust is prescribed to the observed 10-m level maximum wind speed. **d** Same as **a** but for 1200 UTC 26 January 1995. **e** Same as **b** but for 1200 UTC 26 January 1995

application of the Brasseur's method to the observed vertical virtual potential temperature and wind speed profiles produced the observed wind speed at the surface on 0000 UTC 25 January 1995 but too strong wind gust at 1200 UTC. Consequently, the mean value of the turbulence kinetic energy as evaluated on the basis of Eq. 1 using observed profiles was large enough to overcome the mean buoyancy forces to some level in the PBL, and the gust winds were oversimulated as can be seen on the wind speed profile in Fig. 5b.

Figure 5d shows the temperature profiles obtained from a radiosounding at Payerne and computed by the 2-km CRCM on 1200 UTC 26 January 1995 during the windstorm event induced by westerly flows. The simulated surface maximum wind speed, as computed by the 2-km CRCM, overestimates some of the observed hourly maximum wind speed, but on average, underestimates it slightly. The simulated and observed temperature profiles are in a general agreement below 10 km, but differ in the levels below 1,800 m in the PBL; the observed temperature profile is conditionally stable but the simulated one is simulated stable where a temperature inversion is simulated in the lowest level. The simulated LLJ

in Fig. 5e overestimates by 5 ms^{-1} and is closer to the surface than the observed one. The strong vertical shear of the horizontal wind speed component induced TKE values in the column which was large enough to overcome the buoyancy forces. Thus, the gust speed value is identical to the wind speed at 250 m above the surface which exceeds the observed maximum wind speed. This is also visible in Fig. 5c.

Figure 6a shows temperature profiles obtained from a radiosounding at Payerne and computed by the 2-km CRCM on 1200 UTC 17 December 1997 during the southerly flow event that generated a south Foehn in many alpine valleys. During that day, the simulated surface maximum wind speed overestimates many of the observed hourly maximum wind speed (cf. Figure 4b). The simulated and observed temperature profiles are not in good agreement in the PBL; the temperature inversion seen in the sounding below 1,600 m is simulated below 500 m and the 2-km CRCM simulates a more stable atmosphere above the inversion. Figure 6b shows that the LLJ underestimates by 15 ms^{-1} and is simulated 1,500 m closer to the surface than the observed one. The observed vertical shear of the horizontal wind speed component is reproduced stronger on the average by the 2-km CRCM. Consequently the TKE values in the column were then large enough to overcome the buoyancy forces. Thus, the gust speed value simulated above the anemometer level overestimates the observed maximum wind speed at that time. Nevertheless, the gust parameterization scheme performs rather well during that day as shown in Fig. 6c.

Figure 7a plots the temperature profiles obtained from a radiosounding at Payerne and computed by the 2-km CRCM on 1200 UTC 23 November 2005 during a northeasterly flow event inducing the "Bise" from the NE sector. The simulated surface maximum wind speed as computed by the 2-km CRCM fairly reproduced many of the observed hourly maximum wind speed; however, during this day on average, the simulated surface maximum wind speed underestimated a little the observed hourly maximum wind speed (Fig. 4c). The simulated and observed temperature profiles are not in good agreement in the PBL; the temperature inversions seen in the sounding in the PBL are not reproduced in 2-km CRCM simulation where the atmosphere is conditionally stable on the average. Shown in Fig. 7b, the LLJ underestimated by 8 ms^{-1} is simulated 300 m closer to the surface than the observed one. The observed strong vertical shear of the horizontal wind speed component is not well reproduced as strong by the 2-km CRCM. However, the TKE values in the column were then often large enough to overcome the buoyancy forces. Thus, the gust speed value was that of the wind speed at 10 m above the surface corresponded often well to the observed maximum wind speed during that moment as can been seen in Fig. 7c.

5 Discussion

Our results from these three typical storms generally apply to all 24 storms listed in Table 1. Wind outputs are similar to these plotted in Fig. 4, and the simulated pressures are always close to the observed ones, apart from some differences at stations where the altitude difference is significant. Therefore, simulated and observed surface atmospheric pressures vary fairly well in the Swiss Plateau or in rather flat valleys, while R^2 coefficient values are smaller in the Alps and to a lesser extent in the Jura. The wind outputs for the other storms also look similar to the ones plotted for the three storms in Fig. 3, with comparable R^2 determination coefficients. No particular geographical relationship is observed where results may be independent of the altitude difference or the topographic conditions. However, this parameterization does not perform well at high-elevation sites when stations are decoupled from the PBL. This particular 2-km CRCM model setup, including the on-line diagnostic wind gust parameterization, reproduces the hourly maximum wind speed at the anemometer level in a general realistic manner. The hourly maxima were sometimes overestimated but sometimes underestimated with respect to the observed values.

The results shown in the previous section are complemented by an analysis made on a number of other simulated storms (not shown). The analysis, made on the basis of the Payerne station observations, indicates that the static stability, the shear of the horizontal component of the wind velocity, and TKE through the difference Pr−Ri, play a key role in the determination of the maximum wind speed at the anemometer level. Our results show that when the surface maximum wind speed is underestimated by the Brasseur's wind gust parameterization, the model simulates a stronger than observed static stability and a weaker vertical shear of the horizontal wind speed. When the surface maximum wind speed is overestimated by the Brasseur's wind gust parameterization in the 2-km CRCM, the analysis shows that the model simulate a steeper than observed vertical shear of the horizontal wind speed which produces large values of the TKE to overcome the buoyancy forces in the lower layers of the PBL. Consequently, the surface wind gust is that of the wind speed at some height z_p above z_{anem} for which Eq. 1 is satisfied. The analysis also shows that when the hourly maximum wind speeds are underestimated in the 2-km CRCM, the corresponding winds upon applying the gust parameterization scheme to observed profiles at the Payerne aerological station were well reproduced on the average. Therefore, the underestimations in the 2-km CRCM come from the underestimation of the diagnostic formulation of the anemometer-level wind speed that is serving as the lower bound for the gust speed. One may conclude that this wind gust parameterization is rather

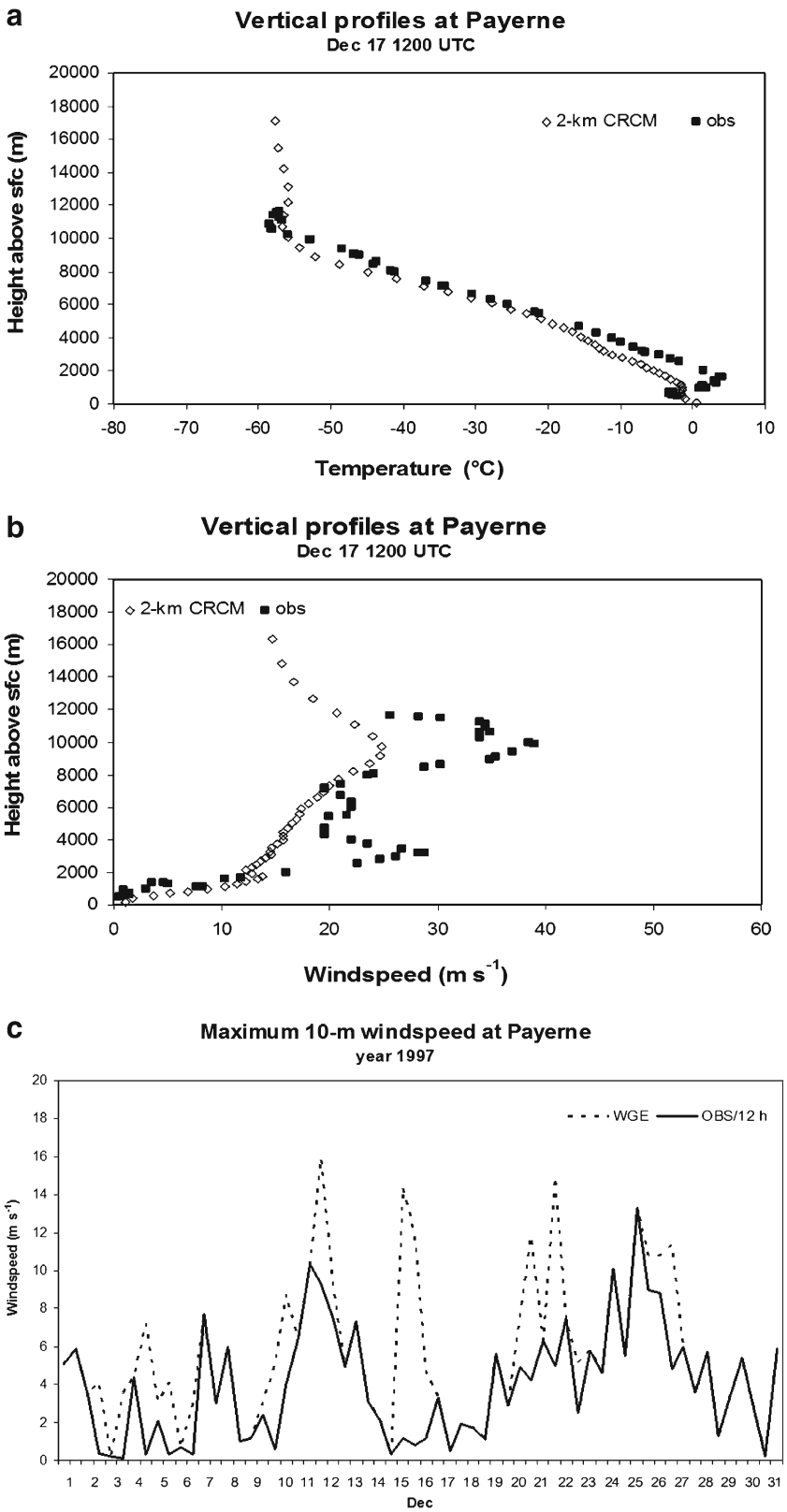

Fig. 6 **a** Same as Fig. 5a but for 1200 UTC 17 December 1997. **b** Same as **a** but for wind speeds. **c** Same as Fig. 5c but for December 1 to 31, 1997

sensitive to the simulated atmospheric flow fields, as well as to the PBL scheme. As reported previously by e.g. Ágústsson and Ólafsson (2009), the accuracy of the method strongly depends on the accuracy of the simulated atmospheric fields in the PBL. In addition, the stability in the lowest model level in the PBL also depends on the surface temperature and

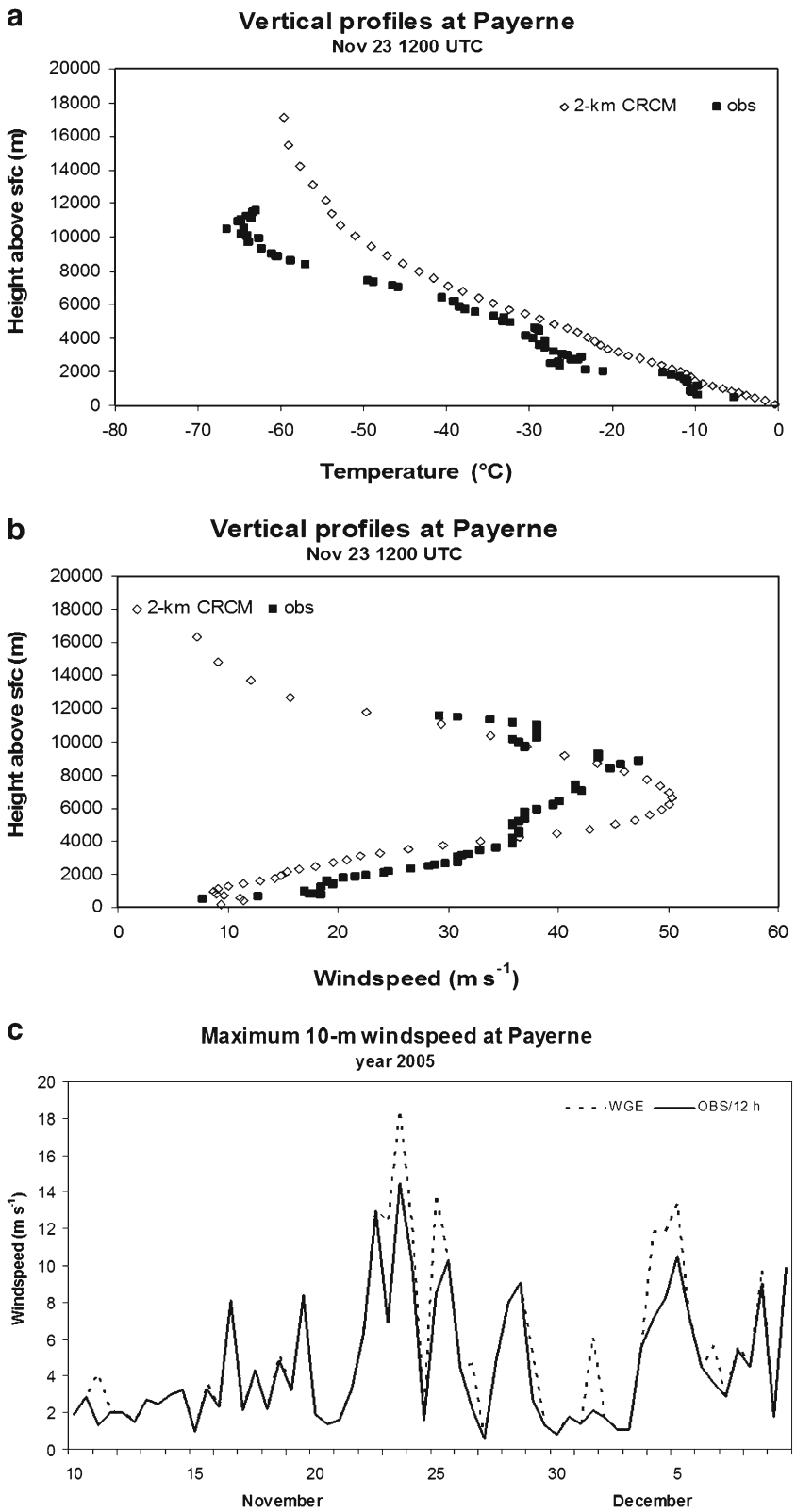

Figure 7 **a** Same as Fig. 5a but for 1200 UTC 23 November 2005. **b** Same as **a** but for wind speeds. **c** Same as Fig. 5c but for 10 November to 9 December 2005

moisture. Thus, the land-surface scheme plays a key role in the reproduction of the wind gusts as shown in Fig. 6a. On the basis of observed vertical profiles (Figs. 5, 6, 7), this parameterization tends to overestimate the observed maximum hourly wind speed at the anemometer level.

6 Conclusions

This paper analyses the ability of the Canadian Regional Climate Model (CRCM) to reproduce a suite of 24 wind storms that occurred over the past 20 years and that were of major relevance for the insurance industry in central European countries, and for Switzerland in particular. Among these major storms are Vivian (27 February 1990), Lothar (26 December 1999) and other secondary storms induced by westerly flows, as well as a number of strong wind South Foehn events induced by southerly flows and "Bise" events induced by north-easterly flows. To run the numerical simulations, NCEP–NCAR reanalysis data is first used as input to drive the CRCM simulations at 60 km. A multiple self-nesting technique is then used to reach 2-km simulations, where the gust parameterisation scheme of Brasseur (2001) is implemented and used to assess the strong winds over the complex topography of Switzerland.

To assess the potential of the model to accurately reproduce the storm events, both synoptic scale and fine-scale comparisons are made with observations. The closest grid points of the CRCM-2 km to each weather station are selected, and the wind speed and pressure outputs are compared to observations recorded by the matching weather stations. Results for the atmospheric surface pressure show that simulated outputs are close to observations, except to these for stations located in mountain areas where difference in altitude is significant. The analysis of the time series of the hourly wind speeds at the anemometer level indicates that model and observed wind gusts have comparable overall behaviours, but differ in details. The discrepancies found between simulated and observed hourly maximum wind speeds may be explained in part by the lack of accuracy of this model setup in reproducing the flow fields in the planetary boundary layer, where the behaviour of the latter, in terms of the static stability (unstable, neutral, stable) can be partially attributed to the performance of the land-surface scheme. This wind gust parameterization should also be modified for high-elevation sites decoupled from the PBL. Consequently, while strong maximum winds are reproduced with some accuracy, a word of caution should be addressed before using these results for a more in-depth evaluation of particular storm damage and employed further as inputs in a storm loss model.

Further tests are thus needed to improve and validate the Brasseur's parameterization in the 2-km CRCM over complex terrain in combination with the current PBL and the land-surface schemes. In particular, the sensitivity of the gust winds to the horizontal and vertical resolution, to the formulation of the surface turbulence parameterization with respect to the values of the roughness height (or neutral drag coefficient) and to the land-surface scheme to compute the surface temperature and moisture. As shown in this study, the model response depends upon the resolved distribution and height of the terrain. Work is underway to modify this parameterization in order to better capture the gusty nature of the wind at highelevation sites over complex topography. This step will warrant a better representation of gust in the current climate and will give much confidence in the representation of extreme winds in a future warmer world.

Acknowledgments The authors would like to thank the Cantons of Geneva, Vaud, Fribourg, Bern and Neuchatel for providing the data of the lake surface temperatures. They are also grateful to the CIPEL and to Dr. Markus Zeh from the Amt für Wasser und Abfall (AWA) for the help they provided to gather the lake temperature data. Authors are also very grateful to Dr. Denis Cohen for his support in reading, checking and commenting the document prior to its submission.

References

Abdella K, McFarlane N (1997) A new second order turbulence closure for the planetary boundary layer. J Atmos Sc 54:1850–1867

Agustsson H, Olafsson H (2004) Mean gust factors over complex terrain. Meteorol Z 13:149–155

Ágústsson H, Ólafsson H (2009) Forecasting wind gusts in complex terrain. Meteorol Atmos Phys 103:173–185. doi:10.1007/s00703-008-0347-y

Alexandru A, de Elia R, Laprise R et al (2009) Sensitivity study of regional climate model simulations to large-scale nudging parameters. Mon Wea Rev 137:1666–1686. doi:10.1175/2008MWR2620.1

Al-Yahyai S, Charabi Y, Gastli A et al (2012) Assessment of wind energy potential locations in Oman using data from existing weather stations. Renew Sustain Energy Rev 14:1428–1436

Antic SR, Laprise BD, de Elía R (2005) Testing the downscaling ability of a one-way nested regional climate model in regions of complex topography. Clim Dyn 23:473–493

Bantle, H. (1989) Program documentation for the Swiss climate data base at the computing centre of ETH Zurich, MeteoSwiss publication, Zurich, Switzerland, 8 pp. www.meteoswiss.ch. Accessed 23 Nov 2012

Barnston AG, Livezey RE (1987) Classification, seasonality and persistence of low-frequency atmospheric circulation patterns. Mon Weather Rev 115:1083–1126. doi:10.1175/1520-0493

Barredo JI (2010) No upward trend in normalised windstorm losses in Europe: 1970–2008. Nat Hazards Earth Syst Sci 10:97–104

Begert M, Schlegel T, Kirchhofer W (2005) Homogeneous temperature and precipitation series of Switzerland from 1864 to 2000. Int J Climatol 25:65–80. doi:10.1002/joc.1118

Bengtsson L, Hodges KI, Roeckner E (2006) Storm tracks and climate change. J Clim 19:3518–3543. doi:10.1175/jcli3815.1

Belŭsić D, Klaić ZB (2004) Estimation of Bora wind gusts using a limited area model. Tellus 56A:296–307

Beniston M, Stephenson DB, Christensen OB et al (2007) Future extreme events in European climate: an exploration of regional climate model projections. Clim Change 81:71–95. doi:10.1007/s10584-006-9226-z

Benoît R, Desgagne M, Pellerin P et al (1997) The Canadian MC2: a semi-Lagrangian, semi-implicit wideband atmospheric model suited for fine scale process studies and simulation. Mon Weather Rev 125:2382–2415

Blackadar AK (1962) Vertical distribution of wind and turbulent exchange in a neutral atmosphere. J Geophys Res 67:3095–3102

Bohle-Carbonell M (1991) Wind and currents-response patterns of Lake Geneva. Ann Geophys-Atmos Hydrospheres and Space Sci 9:82–90

Born K, Ludwig P, Pinto JG (2012) Wind gust estimation for Mid-European winter storms: towards a probabilistic view. Tellus A 64:17471. doi:10.3402/tellusa.v64i0.17471

Brasseur O (2001) Development and application of a physical approach to estimating wind gusts. Mon Weather Rev 129:5–25

Brasseur O, Gallée H, Boyen H et al (2002) Reply. Mon Weather Rev 130:1936–1942

Burk SD, Thompson WT (2002) Comments on "Development and application of a physical approach to estimating wind gusts". Mon Weather Rev 130:1933–1935

Bresch, D. N., Bisping, M., and Lemecke, G. (2000) Storm over Europe: an underestimated risk, Swiss Reinsurance Company, 27 pp. www.swissre.com. Accessed 23 Nov 2012

Caya D, Laprise R (1999) A semi-implicit semi Lagrangian regional climate model: the Canadian RCM. Mon Weather Rev 127:341–362

Champeaux JL, Masson V, Chauvin R (2005) ECOCLIMAP: a global database of land surface parameters at 1 km resolution. Meteorol Appl 12:29–32. doi:10.1017/S1350482705001519

Della-Marta PM, Liniger MA, Appenzeller C et al (2010) Improved estimates of the European winter windstorm climate and the risk of reinsurance loss using climate model data. J Appl Meteorol Climatol 49:2092–2120. doi:10.1175/2010JAMC2133.1

Denis B, Laprise R, Caya D et al (2002) Downscaling ability of one-way-nested regional climate models: the Big-Brother Experiment. Clim Dyn 18:627–646

Durst CS (1960) Wind speeds over short period of time. Meteor Mag 89:181–187

Etienne C, Lehmann A, Goyette S et al (2010) Spatial predictions of extreme wind speeds over Switzerland using generalized additive models. J Appl Meteor Climatol 49:1956–1970. doi:10.1175/2010jamc2206.1

Fischer-Bruns I, von Storch H, Gonzalez-Rouco JF et al (2005) Modelling the variability of midlatitude storm activity on decadal to century time scales. Clim Dyn 25:461–476. doi:10.1007/S00382-005-0036-1

Furger M (1992) The radiosoundings of Payerne: aspects of the synoptic-dynamic climatology of the wind field near mountain ranges. Theor Appl Climatol 45:3–17. doi:10.1007/bf00865989

Goyette S, McFarlane NA, Flato GM (2000) Application of the Canadian Regional Climate Model to the Laurentian Great Lakes region: implementation of a lake model. Atmos Ocean 38:481–503

Goyette S, Beniston M, Caya D et al (2001) Numerical investigation of an extreme storm with the Canadian Regional Climate Model: the case study of windstorm Vivian, Switzerland, February 27, 1990. Clim Dyn 18:145–178

Goyette S, Brasseur O, Beniston M (2003) Application of a new wind gust parameterisation. Multi-scale case studies performed with the Canadian RCM. J Geophys Res 108(D13):4374–4390

Goyette S (2008) Development of a model-based high resolution extreme surface wind climatology for Switzerland. Nat Hazards 44:329–339. doi:10.1007/s11069-007-9130-5

Heneka, P., and Ruck, B. (2004) Development of a storm damage risk map of Germany—a review of storm damage functions, International Conference for Disasters and Society, Karlsruhe. http://www.cedim.de. Accessed 23 Nov 2012

Heneka P, Hofherr T, Ruck B et al (2006) Winter storm risk of residential structures-model development and application to the German state of Baden-Wuerttemberg. Nat Hazards Earth Syst Sci 6:721–733

Henne S, Furger M, Prevot ASH (2005) Climatology of mountain venting-induced elevated moisture layers in the lee of the Alps. J Appl Meteor 44:620–633. doi:10.1175/jam2217.1

Hoinka KP (1985) Observation of the air-flow over the Alps during a Foehn event. Q J R Meteorol Soc 111:199–224. doi:10.1256/smsqj.46708

Holton JR (2004) An Introduction to Dynamic Meteorology, 4th edn. Academic Press, London, 535 pages

Jungo P, Goyette S, Beniston M (2002) Daily wind gust speed probabilities over Switzerland and according to three types of synoptic circulation. Int J Climatol 22:485–499

Kalnay E, Kanamitsu M, Kistler R et al (1996) The NCEP/NCAR 40-year reanalysis project. Bull Amer Meteorol Soc 77:437–471

Klawa M, Ulbrich U (2003) A model for the estimation of storm losses and the identification of severe winter storms in Germany. Nat Hazards Earth Syst Sci 3:725–732

Lambert S, Sheng J, Boyle J (2002) Winter cyclone frequencies in thirteen models participating in the Atmospheric Model Intercomparison Project (AMIP 1). Clim Dyn 19:1–16

Lambert SJ, Fyfe JC (2006) Changes in winter cyclone frequencies and strengths simulated in enhanced greenhouse warming experiments: results from the models participating in the IPCC diagnostic exercise. Clim Dyn 26:713–728. doi:10.1007/s00382-006-0110-3

Laprise R, Caya D, Giguere M et al (1998) Climate and climate change in Western Canada as simulated by the Canadian Regional Climate Model. Atmos Ocean 36:119–167

Laprise R, Caya D, Frigon A et al (2003) Current and perturbed climate as simulated by the second-generation Canadian Regional Climate Model (CRCM-II) over northwestern North America. Clim Dyn 21:405–421

Leckebusch GC, Ulbrich U (2004) On the relationship between cyclones and extreme windstorm events over Europe under climate change. Glob Planet Chang 44:181–193. doi:10.1016/j.gloplacha.2004.06.011

Leckebusch G, Koffi B, Ulbrich U et al (2006) Analysis of frequency and intensity of European winter storm events from a multi-model perspective, at synoptic and regional scales. Clim Res 31:59–74

Masson V, Champeaux J-L, Chauvin F et al (2003) A global database of land surface parameters at 1-km resolution in meteorological and climate models. J Clim 16(9):1261–1282

Martynov A, Sushama L, Laprise R et al (2012) Interactive lakes in the Canadian Regional Climate Model, version 5: the role of lakes in the regional climate of North America. Tellus A 64:16226. doi:10.3402/tellusa.v64i0.16226

McFarlane NA, Boer GJ, Blanchet J-P et al (1992) The Canadian climate centre second generation general circulation model and its equilibrium climate. J Clim 5:1013–1044

Mellor GL, Yamada T (1974) Hierarchy of turbulence closure models for planetary boundary-layers. J Atmos Sc 31:1791–1806. doi:10.1175/1520-0469

Mellor GL, Yamada T (1982) Development of a turbulence closure model for geophysical fluid problems. Rev Geophys Space Phys 20:851–875. doi:10.1029/RG020i004p00851

Mitchell JFB, Wilson CA, Price C (1985) On the Specification of surface fluxes in coupled atmosphere–ocean general circulation models. Chap. 18. Elsevier Oceanogr Ser 40:249–262

MunichRe (2001) Winter storms in Europe (II)–Analysis of 1999 losses and loss potentials, Munich Reinsurance Company. www.munichre.com. Accessed 23 Nov 2012

Nielsen, N. W. and Petersen, C. (2001) Calculation of wind gusts in DMI-HIRLAM. Danish Meteorological Institute, SC. Report 01–03, Copenhagen, 32 pp. http://www.dmi.dk/dmi/sr01-03.pdf. Accessed 23 Nov 2012

Ólafsson H, Agustsson H (2007) The freysnes downslope windstorm. Meteorol Z 16:123–130. doi:10.1127/0941-2948/2007/0180

Pielke RA (2002) Mesoscale meteorological modelling. Academic Press, London, 676 pages

Pinto JG, Zacharias S, Fink AH et al (2009a) Factors contributing to the development of extreme North Atlantic cyclones and their

relationship with the NAO. Clim Dyn 32:711–737. doi:10.1007/s00382-008-0396-4

Pinto JG, Neuhaus CP, Krüger A et al (2009b) Assessment of the wind gust estimates method in mesoscale modelling of storm events over West Germany. Meteorol Z 18:495–506. doi:10.1127/0941-2948/2009/0402

Plummer DA, Caya D, Frigon A et al (2006) Climate and climate change over North America as simulated by the Canadian RCM. J Clim 19:3112–3132. doi:10.1175/JCLI3769.1

Pfister C (1999) Wetternachhersage, 500 Jahre Klimavariationen und Naturkatastrophen. Paul Haupt Verlag, Bern, Stuttgart, Wien, p 304

Raible CC, Della-Marta PM, Schwierz C et al (2008) Northern hemisphere extra-tropical cyclones: a comparison of detection and tracking methods and different reanalyses. Mon Weather Rev 136:880–897. doi:10.1175/2007mwr2143.1

Schiesser HH, Pfister C, Bader J (1997) Winter storms in Switzerland North of the Alps 1864/1865-1993/1994. Theor Appl Climatol 58:1–19

Schmith T, Kaas E, Li T-S (1998) Northeast Atlantic winter storminess 1875–1995 re-analysed. Clim Dyn 14:529–536

Schraft, A., Durand, E., and Hausmann, P. (1993) Storms over Europe: losses and scenarios, Swiss Reinsurance Company, 28 pp. www.swissre.com. Accessed 23 Nov 2012

Schüepp M (1978) Klimatologie der Schweiz. Band III. In Beiheft zu den Annalen der Schweizerischen Meteorologischen Anstalt, Zurich, p 89

Schüepp M, Schiesser HH, Huntrieser H et al (1994) The windstorm "Vivian" of 27 February 1990: about the meteorological development, wind forces and damage situation in the forest of Switzerland. Theor Appl Climatol 49:183–200

Schulz, J.-P. (2008) Revision of the turbulent gust diagnostics in the COSMO model. COSMO Newslett. 8: 17–22. www.cosmo-model.org. Accessed 23 Nov 2012

Schwierz C, Kollner-Heck P, Mutter EZ et al (2010) Modelling European winter wind storm losses in current and future climate. Clim Change 101:485–514. doi:10.1007/s10584-009-9712-1

Stephenson DB, Wanner H, Broennimann S et al (2002) The history of scientific research on the North Atlantic Oscillation. In: Hurrell JW, Kushnir Y, Ottersen G, Visbeck M (eds) The North Atlantic Oscillation: climatic significance and environmental impact, Geophysical Monograph 134. American Geophysical Union, Washington, pp 37–50

von Storch H, Weisse R (2008) Regional storm climate and related marine hazards in the Northeast Atlantic. In: Diaz HF, Murnane RJ (eds) Climate extremes and society. Cambridge University Press, Cambridge, p 340

Thorarinsdottir TL, Johnson MS (2012) Probabilistic wind gust forecasting using non-homogeneous Gaussian regression. Mon Wea Rev 140:889–897. doi:10.1175/MWR-D-11-00075.1

Tveito, O. E., Wegehenke, M., van der Wel, F., and Dobesch, H. (2008) The use of geographic information systems in climatology and meteorology, Office for Official Publications of the European Communities, 245 pp

Ulbrich U, Leckebusch GC, Pinto JG (2009) Cyclones in the present and future climate: a review. Theor Appl Climatol 96:117–131. doi:10.1007/s00704-008-0083-8

Usbeck T, Wohlgemuth T, Dobbertin M et al (2010) Increasing storm damage to forests in Switzerland from 1858 to 2007. Agric For Meteorol 150:47–55. doi:10.1016/j.agrformet.2009.08.010

Wanner H, Furger M (1990) The Bise—climatology of a regional wind north of the Alps. Meteorol Atmos Phys 43:105–115. doi:10.1007/bf01028113

Wang XL, Zwiers FW, Swail VR et al (2009) Trends and variability of storminess in the Northeast Atlantic Region, 1874–2007. Clim Dyn 33:1179–1195. doi:10.1007/s00382-008-0504-5

WASA Group (1998) Changing waves and storms in the Northeast Atlantic. Bull Am Met Soc 79:741–760

Wieringa J (1973) Gust factors over open water and built up country. Bound Layer Meteor 3:424–441

Wilson MF, Henderson-Sellers A (1985) A global archive of land cover and soils data for use in general circulation climate models. J Climatol 5:119–143